

This is post-print version of the paper published in:

***Mater. Chem. Phys.* 163 (2015); 453 - 459**

DOI: [10.1016/j.matchemphys.2015.07.065](https://doi.org/10.1016/j.matchemphys.2015.07.065)

Effect of lattice disorder on the thermal conductivity of ZnBeSe, ZnMgSe and ZnBeMgSe crystals

K. Strzalkowski

Institute of Physics, Faculty of Physics, Astronomy and Informatics, Nicolaus Copernicus University, Grudziadzka 5, 87-100 Torun, Poland
skaroll@fizyka.umk.pl

Abstract

Zn_{1-x-y}Be_xMg_ySe mixed crystals investigated in this work were grown from the melt by the high pressure high temperature modified Bridgman method in the range of composition $0 < x, y < 0.33$. Photopyroelectric (PPE) calorimetry in the back (BPPE) and front (FPPE) configuration was applied for thermal investigation of solid samples. The thermal diffusivity and effusivity of investigated crystals were derived from the experimental data. Since dynamic thermal parameters are connected with each other, thermal conductivity of the specimens was calculated from theoretical dependencies between them. The influence of the beryllium (x) and magnesium (y) content on thermal properties of these crystals have been presented and discussed. Order-disorder effects observed for these materials previously have been also taken into account. Finally, thermal diagrams, i.e. thermal conductivity versus composition were presented and discussed applying model given by Sadao Adachi.

Keywords: Alloys; Semiconductors; Crystal growth; Thermal conductivity; Thermal properties

1 Introduction

Broadband solid solutions of II-VI compounds are of interest not only because of cognitive considerations, but also as potential materials for practical applications in modern optoelectronics. Their physical properties are poorly examined primarily due to the difficult technology for their preparation. II-VI mixed crystals are still interested materials in modern electronics, optics and spintronics, primarily due to possibility of tuning material properties like energy gap or lattice constant. In general, following topics are now intensively studied: solar cells [1], infrared, ultraviolet, X- and γ -ray photodetectors [2-4], magnetic materials [5], ZnO based devices [6] and light-emitting structures [7].

The phenomenon of the transport of the heat in semiconductor materials is a complex matter, particularly in the case of mixed ternary and quaternary crystals. It depends on the composition, structural characteristics and the preparation process. From application point of view the most important parameters characterizing materials used in electronics are the thermal conductivity and diffusivity. The knowledge about them is required in the design and construction of semiconductor devices. Determination of thermal parameters of completely new materials is therefore very important.

Photothermal methods are widely used in studying thermal properties of solid samples [8-11]. Among them, photopyroelectric technique is fast, simple, high sensitivity and non-destructive experimental method [11]. Basically, in PPE technique the experiment can be carried out in two measurement configurations. In the back mode an incident radiation illuminates the sample placed onto the sensor. On the other hand, in the front configuration the sensor is being excited and the sample acts like kind of heat-sink placed on the opposite side of the detector. Thermal diffusivity and effusivity can be obtained in the back and in front detection configuration, respectively. Thermal conductivity can be then easily calculated.

The aim of this work is to characterize the thermal properties (effusivity, diffusivity and conductivity) of the selected $Zn_{1-x-y}Be_xMg_ySe$ mixed semiconducting crystals as a function of the composition and finding the correlation between the received thermal parameters and other properties of the materials. The results will be analyzed, among others, in the model proposed by Adachi [12] for mixed semiconductor crystals. Adachi used simply relation for thermal resistivity of semiconducting alloys and successfully applied it to several IV and III-V alloys like: C_xSi_{1-x} , Si_xGe_{1-x} , $Al_xGa_{1-x}As$, $Al_xGa_{1-x}N$, $Ga_xIn_{1-x}As$ or $Ga_xIn_{1-x}Sb$. Since mechanism of thermal conductivity in II-VI materials investigated in this work is mainly due to lattice contribution, their thermal properties can be also analyzed in given model.

2 Experimental set up and sample preparation

2.1 Samples description

Investigated in this work $Zn_{1-x-y}Be_xMg_ySe$ crystals were produced by the high temperature and high pressure modified vertical Bridgman method with different Be and Mg concentrations under argon overpressure of about 150 atm. ZnSe (6N, Koch-Light), Be (99.8%) and Mg (99.8%) powders mixed together in stoichiometric proportion were used as a starting materials. To reduce the concentration of cation vacancies starting powders were prepared with little superiority of Be and Mg. Such mixtures were put into graphite crucible

and kept at temperature of about 1850 K for a few hours and then moved out from the heating zone at a speed of 2.4 mm/h. More details concerning technical data of this process were published previously [13]. Produced crystal rods were of 1 cm in diameter and up to few cm in length. Obtained crystals were cut perpendicular to the growth axis into about 1-1.5 mm slices, which were not orientated along any crystallographic plane. The plates were first mechanically ground (Al_2O_3 powder, 10 μm) and then polished with diamond paste (0.1-1 μm). Such prepared specimens were investigated in this work.

Results of composition and structure of investigated crystals are reported in Table 1, they all were taken from papers published previously for these compounds.

X-ray investigations showed that $\text{Zn}_{1-x}\text{Be}_x\text{Se}$ samples exhibited a single sphalerite phase (zinc blende, ZB). The Be content was determined for each sample with a typical accuracy of $\pm 0.5\%$ from the lattice constant measured by x-ray diffraction assuming Vegard's rule [14].

The composition of the ternary $\text{Zn}_{1-x}\text{Mg}_x\text{Se}$ crystals was determined with a Jeol JXA-50A electron probe micro-analyzer. Phase analysis was performed in a step scanning mode using a standard x-ray Bragg-Brentano powder diffractometer and Ni-filtered Cu KLY radiation.

Powder diffraction analysis showed that samples with $x=0.06$ and 0.12 are single-phase sphalerite type with a trace content of the hexagonal modification. Samples with higher magnesium content exhibit wurtzite (W) type structure [15].

Table 1 The composition and thickness of $\text{Zn}_{1-x-y}\text{Be}_x\text{Mg}_y\text{Se}$ plates

Starting content		Results of analysis		Structure	Thickness [mm]
x	y	x	y		
0	0	-	-	ZB	1.18
0.05	0	0.04	0	ZB	1.21
0.1	0	0.1	0	ZB	1.48
0.15	0	0.17	0	ZB	1.18
0.2	0	0.26	0	ZB	1.18
0	0.05	0	0.06	ZB+W	1
0	0.1	0	0.12	ZB+W	0.97
0	0.2	0	0.22	W	1.26
0	0.3	0	0.33	W	1
0.04	0.14	0.04	0.12	ZB	1.35
0.06	0.26	0.06	0.22	ZB+W	1.15

Zn, Mg and Se concentrations in quaternary $\text{Zn}_{1-x-y}\text{Be}_x\text{Mg}_y\text{Se}$ were determined with the SEM/EDS method using Quantax 200 X-ray spectrometer and EDX XFlash 4010 detector. The Be content was calculated assuming that the sum of cation (Zn, Mg, Be) contents (in atomic percent) is equal to that of Se anion. X-ray investigations showed that both samples $\text{Zn}_{0.84}\text{Be}_{0.04}\text{Mg}_{0.12}\text{Se}$ and $\text{Zn}_{0.72}\text{Be}_{0.06}\text{Mg}_{0.26}\text{Se}$ were uniform in composition. First specimen exhibits a single sphalerite phase and the second one sphalerite with trace of wurtzite [16].

2.2 Experimental systems

PPE standard experimental setup for front and modified for back measurement detection configuration was used [17]. It consisted of a 300 mW power blue diode laser ($\lambda=405$ nm), a 0.4 mm thick LiTaO₃ detector, provided with CrAu electrodes and a SR850 dual-phase lock-in amplifier. The excitation radiation was modulated electronically via lock-in TTL output. The laser spot was extended up to 3 mm to satisfy one dimensional model of the heat propagation through the sample. In PPE method an optically opaque sample is placed onto the sensor. Exciting radiation impinges the sample or the sensor, depending on the measurement configuration (see Fig. 1).

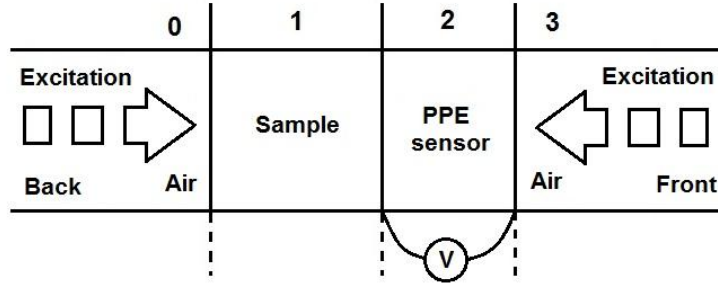


Fig. 1 Model of the experimental cell in the back and front configuration for the PPE method

A thin layer of ethylene glycol ($\alpha=9.36 \times 10^{-8} \text{ m}^2 \cdot \text{s}^{-1}$ and $e=814 \text{ W} \cdot \text{s}^{1/2} \cdot \text{m}^{-2} \cdot \text{K}^{-1}$) served as a coupling fluid between the sample and the sensor. Thermal diffusivity measurement of solid samples in back PPE configuration requires thin layer of coupling fluid between the sample and the sensor. This always leads to underestimation of obtained results. However, it was shown, that main source of this error is the thickness of the coupling fluid and this undesired effect can be minimized applying simply experimental modification [17]. In modified setup the sample is stick to the sensor with ethylene glycol and some pushing force is applied to it. Thanks to that the influence of the thickness of the liquid on thermal diffusivity values has been reduced [17,18]. The modulation frequency of the excitation source was changed in the range 1 to 15 Hz and 5 to 45 Hz in case of back and front mode, respectively. For both BPPE and FPPE configuration normalization procedure with empty sensor was applied. Binary ZnSe crystal ($x,y=0$) was used for reference purpose as material with known thermal properties. All the measurements have been performed at room temperature and were computer-controlled.

3 Theory

The cell configuration in PPE technique consists of four-layers presented in Fig. 1. Assuming a perfect thermal contact between the sample and the sensor and the one-dimensional model of the heat propagation through the whole system, the complex PPE signal in back configuration is given by [19-22]:

$$V = \frac{2V_0 e^{-\sigma_s L_s}}{b_{sp} + 1} \frac{1 - e^{-2\sigma_p L_p}}{1 + R_{sp} e^{-2\sigma_p L_p} - (R_{sp} + e^{-2\sigma_p L_p}) e^{-2\sigma_s L_s}} \quad (1)$$

In Eq. (1) V_0 is an instrumental factor, ij represents s and p layers of the detection cell, respectively, $R_{ij} = (b_{ij}-1)/(b_{ij}+1)$ is the reflection coefficient of the thermal wave at ij interface, $b_{ij} = e_i/e_j$ and e is thermal effusivity, $\sigma_i = (1+i)a_i$ is the complex diffusion coefficient, a_i is the reciprocal of the thermal diffusion length μ_i , $a_i = 1/\mu_i$, $\mu_i = (2\alpha_i/\omega)^{1/2}$, ω is the angular modulation frequency and L_i is the thickness of the layer i . In order to eliminate the instrumental factor V_0 was eliminated applying empty sensor normalization procedure [21,22]. Assuming thermally thick regime for both the detector and the sample ($\mu_i \ll L_i$), the complex signal can be separate into amplitude (Eq. (2)) and phase (Eq. (3)) [21,22]:

$$\ln|V_n| = \ln \frac{2}{b_{sp} + 1} - L_s \left(\frac{\omega}{2\alpha_s} \right)^{1/2} \quad (2)$$

$$\Theta_n = \Theta_0 - L_s \left(\frac{\omega}{2\alpha_s} \right)^{1/2} \quad (3)$$

One can calculate the thermal diffusivity of the sample by using the amplitude and/or the phase of the complex signal. However, the amplitude is affected by external factors such as laser-intensity fluctuations and the roughness of the surface, whereas the phase is being independent on these external factors. For this reason, the thermal diffusivity was calculated according to Eq. (3) using phase-lag method [21,22]:

$$\alpha_s = \frac{L_s^2 \pi}{a^2} \quad (4)$$

where a is the slope of the phase graph.

In the front measurement configuration the incident radiation hits directly the sensor. The complex signal in such a case after normalization to the empty detector can be given by [21]:

$$V_n = \frac{1 - e^{-\sigma_p L_p} + R_{sp} (e^{-2\sigma_p L_p} - e^{-\sigma_p L_p})}{1 + R_{sp} e^{-2\sigma_p L_p}} \quad (5)$$

Eq. (5) can be simplified considering assumption that $\mu_p \ll L_p$ (thermally thick detector):

$$V_n = 1 - (1 + R_{sp}) e^{-\sigma_p L_p} \quad (6)$$

From Eq. (6) one can get the amplitude (Eq. (7)) and the phase (Eq. (8)) of the complex signal:

$$|V_n| = \sqrt{[(1 + R_{sp}) e^{-a_p L_p} \sin(a_p L_p)]^2 + [1 - (1 + R_{sp}) e^{-a_p L_p} \cos(a_p L_p)]^2} \quad (7)$$

$$\Theta_n = \arctan \frac{(1 + R_{sp}) e^{-a_p L_p} \sin(a_p L_p)}{1 - (1 + R_{sp}) e^{-a_p L_p} \cos(a_p L_p)} \quad (8)$$

If the sample is known one can determine thermal properties of the detector. For phase normalized with empty sensor signal true is [21]:

$$\frac{L_p}{\mu_p} = \pi \Rightarrow \alpha_p = \frac{L_p^2 f_o}{\pi} \quad (9)$$

where f_o is frequency, where phase is crossing zero and becomes negative.

It is well known, that thermal parameters are connected with each other. Thermal diffusivity is given by [23]:

$$\alpha = \frac{k}{\rho C} \quad (10)$$

where: k is thermal conductivity, ρ is density and C is specific heat capacity.

On the other hand, thermal effusivity can be expressed as:

$$e = (k\rho C)^{1/2} \quad (11)$$

Using both expressions one can eliminate ρC factor and calculate then thermal conductivity from simple relation:

$$k = e\alpha^{1/2} \quad (12)$$

Lattice thermal conductivity in the case of semiconductor alloys requires taking into account a contribution, which is the result of a random distribution of constituent atoms in sublattice sites. A phenomenological model of the lattice thermal conductivity for semiconductor alloys was first proposed by Abeles [24]. However, Adachi [25,12] showed that the thermal resistivity $W(x)$ for ternary $A_xB_{1-x}C$ alloy can be described by simple expression:

$$W(x) = xW_{AC} + (1-x)W_{BC} + x(1-x)C_{A-B} \quad (13)$$

where: W_{AC} and W_{BC} are binary thermal resistivities and C_{A-B} is a contribution arising from the lattice disorder. Eq. (13) can be easily transferred into lattice thermal conductivity $K(x)$:

$$K(x) = \frac{1}{W(x)} = \frac{1}{xW_{AC} + (1-x)W_{BC} + x(1-x)C_{A-B}} \quad (14)$$

4 Experimental results

Specimens investigated in this work in the back PPE configuration were measured using modified experimental setup, described in [17]. Phase characteristics of all samples as a function of the square root of the modulation frequency multiplied by the thickness of the

samples are presented in Fig. 2. Given results are independent on the thickness of the samples and were ordered ascending according to the slope of the phase. Consequently, the thermal diffusivity values systematically decrease for presented series of $Zn_{1-x-y}Be_xMg_ySe$ crystals.

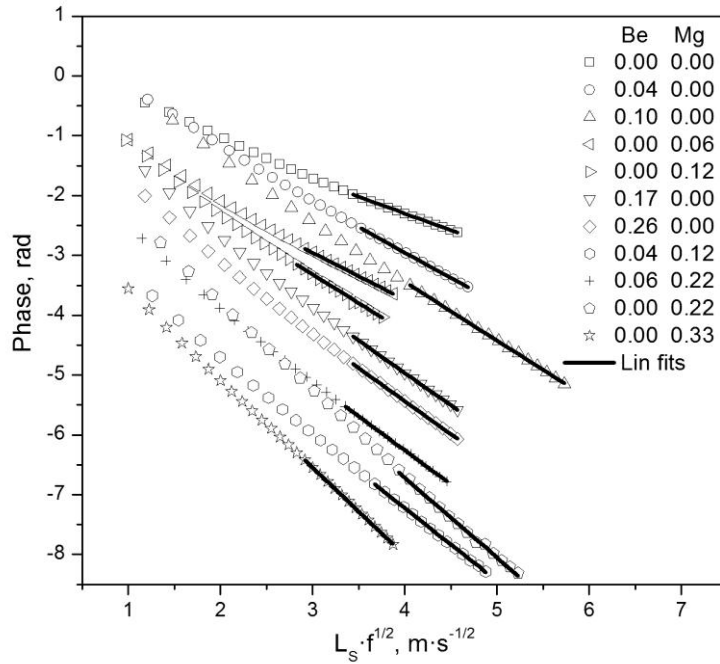


Fig. 2 The BPPE phases in radians of $Zn_{1-x-y}Be_xMg_ySe$ crystals as a function of the square root of the modulation frequency multiplied by the thickness of the sample, points are experimental data and lines are linear fits

Since for low frequency regime the sample and the sensor are thermally thin (thermal wave propagating along the layer is not attenuated at least e times) nonlinear behavior of the phase can be seen. For 1.18 mm thick ZnSe sample ($\alpha = 9.85 \times 10^{-6} \text{ m}^2 \cdot \text{s}^{-1}$) the thermal diffusion length is comparable with its thickness at 2 Hz. Also 0.5 mm thick LiTaO₃ detector with diffusivity of about $1.4 \times 10^{-6} \text{ m}^2 \cdot \text{s}^{-1}$ [26] starts to be thermally thick at similar modulation frequency. Almost all other samples are thermally thick at lower frequencies and consequently the signal coming out from the sensor start to be noisy already at 15 Hz. Consequently, linear fits were performed starting from 6 Hz, where both the sample and the detector are thermally thick. Linear fits were performed applying least square method with R^2 statistical determination coefficient of the order of 0.999996. Thermal diffusivity of the investigated crystals was calculated according to Eq. (4).

PPE technique in the front measurement configuration was applied in order to obtain thermal diffusivity of the investigated materials. The modulation frequency was varying from 5 to 45 Hz, so the sample and the sensor have become thermally thick. Fig. 3a presents phase characteristics of selected $Zn_{1-x}Mg_xSe$ specimens as a function of modulation frequency, points refer to measured data, and lines are best fits obtained with least square method using Eq. (8). The coefficient of determination, denoted R^2 , for $Zn_{0.94}Mg_{0.06}Se$ example crystal can be found in Fig. 3b. Given curve series obtained for $Zn_{1-x}Mg_xSe$ samples are ordered according to decreasing diffusivity value. One can see that all curves are crossing zero phase point for more or less the same modulation frequency. According to the theory [21], one can

state that measurement and normalization procedure were carried out properly. This point can be also used to obtain thermal properties of the sensor, if necessary. In this work following parameters of the LiTaO₃ detector were used: $\alpha_p=1.36 \times 10^{-6} \text{ m}^2 \cdot \text{s}^{-1}$ and $e_p= 3660 \text{ W} \cdot \text{s}^{1/2} \cdot \text{m}^{-2} \cdot \text{K}^{-1}$ [26]. Fig. 3b presents phase characteristic of example Zn_{0.94}Mg_{0.06}Se crystal as a function of modulation frequency. The best fit of Eq. (8) obtained with least square method is also displayed in Fig. 3b. The error arising from the fitting procedure is given in inset. The minimum observed in error graph corresponds to the value of the thermal effusivity of the investigated sample.

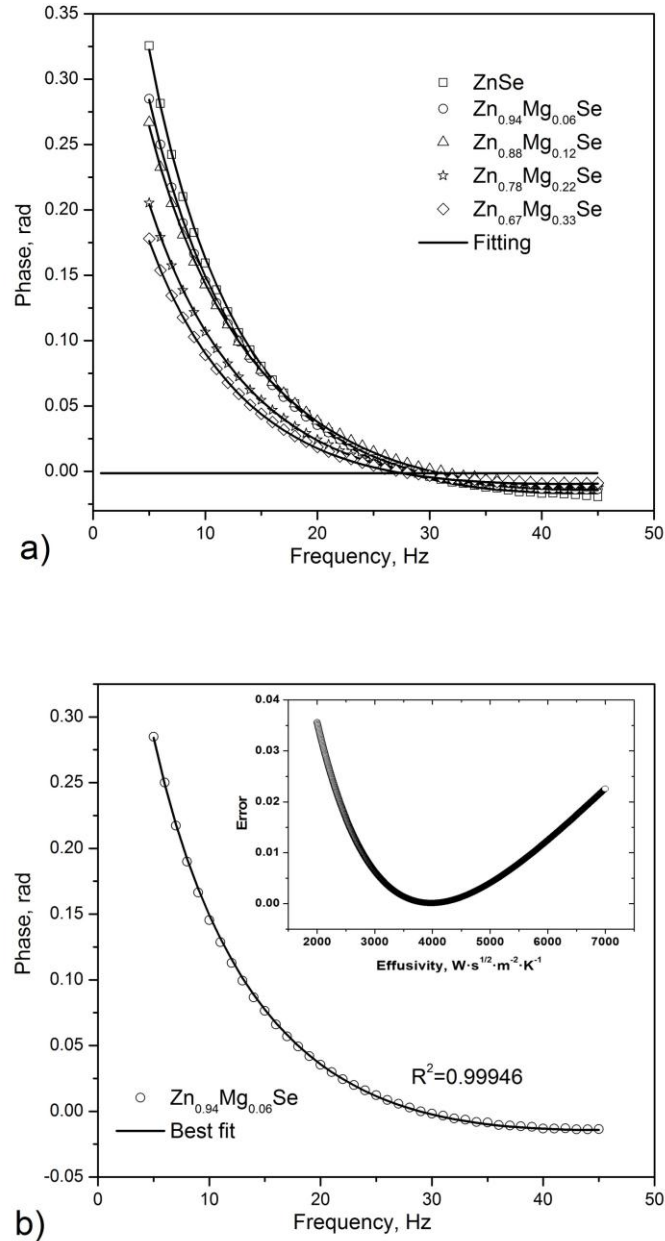


Fig. 3 Phase characteristics of selected Zn_{1-x}Mg_xSe crystals as a function of modulation frequency (a), points refer to measured data, lines are best fits obtained with least square method using Eq. (8). Example fit for Zn_{0.94}Mg_{0.06}Se crystal (b) and the error of the fitting procedure (see inset) was also displayed in

It was mentioned, that thermal parameters are connected with each other by simple relations. Using thermal parameters obtained from experiment, thermal conductivity of the investigated crystals was calculated according to Eq. (12). Complete set of obtained in this work thermal parameters of all investigated specimens is presented in Table 2.

Thermal diffusivity and effusivity values are given as average values from three independent measurements with standard deviation as uncertainty. Uncertainties of the thermal conductivity were calculated using total differential method as simply average errors taking into account thermal diffusivity and effusivity errors. The experimental reproducibility leads to the thermal conductivity uncertainty of the order of 0.5-1.5%, depending on the sample. The thickness of the specimens was measured with a micrometer with an accuracy of 10 μm , which produces additional uncertainty of about 0.2-0.3%. The systematic error connected with the presence of coupling fluid in case of thermal diffusivity [18] and effusivity can be estimated as 3-4%. One can conclude that final uncertainty of the thermal conductivity value is of the order of 5-6%.

5 Discussion

Thermal conductivity of reference ZnSe crystal is smaller than given in literature ($0.19 \text{ W}\cdot\text{cm}^{-1}\cdot\text{K}^{-1}$, [27,28]), however the difference is not large. Observed discrepancy can be explained by two facts: (i) sensitivity of thermal properties on the fabrication process and quality of the crystal structure, (ii) presence of coupling fluid at sample/sensor interface.

Table 2 Thermal parameters of the investigated $\text{Zn}_{1-x-y}\text{Be}_x\text{Mg}_y\text{Se}$ crystals

x	y	Thermal diffusivity ($\text{m}^2\cdot\text{s}^{-1}$) $\times 10^{-6}$	Thermal effusivity ($\text{W}\cdot\text{s}^{1/2}\cdot\text{m}^{-2}\cdot\text{K}^{-1}$)	Thermal conductivity ($\text{W}\cdot\text{cm}^{-1}\cdot\text{K}^{-1}$) $\times 10^2$
0	0	9.846 \pm 0.030	5633.3 \pm 20.2	17.676 \pm 0.09
0.04	0	4.333 \pm 0.042	3851.7 \pm 48.0	8.018 \pm 0.137
0.10	0	3.301 \pm 0.018	3333.3 \pm 10.4	6.056 \pm 0.035
0.17	0	2.691 \pm 0.013	2693.3 \pm 30.6	4.418 \pm 0.061
0.26	0	2.558 \pm 0.012	2686.7 \pm 28.4	4.297 \pm 0.055
0	0.06	5.080 \pm 0.014	4041.7 \pm 56.2	9.109 \pm 0.139
0	0.12	3.560 \pm 0.046	3288.3 \pm 35.1	6.204 \pm 0.106
0	0.22	2.122 \pm 0.009	2328.3 \pm 22.5	3.392 \pm 0.040
0	0.33	1.444 \pm 0.017	1903.3 \pm 15.3	2.287 \pm 0.032
0.04	0.12	2.555 \pm 0.031	2688.3 \pm 29.3	4.297 \pm 0.073
0.06	0.22	2.466 \pm 0.047	2523.3 \pm 27.5	3.962 \pm 0.081

One can see in Table 2, that added magnesium and beryllium to the alloy lead to decreasing of all thermal parameters of the specimens. In our opinion this effect is mainly due to the difference in atomic radius of the components and, as the consequence the disorder is introduced into the crystal structure. Similar behavior was observed previously for $\text{Cd}_{1-x-y}\text{Zn}_x\text{Mg}_y\text{Se}$ mixed compounds [29]. Dumcenco et al. [30] carried out an optical characterization of two wurtzite $\text{Cd}_{1-x-y}\text{Zn}_x\text{Mg}_y\text{Se}$ crystalline alloys by temperature dependent photoreflectance (PR) and contactless electroreflectance (CER). The derived value of the

strength of the exciton-LO phonon coupling for investigated samples was larger than that of Mg free samples. This phenomenon has been attributed to the larger deformation of interaction potential, which might account for a significant fraction of the carriers-phonons coupling. Similar investigations were performed by the same authors for $Zn_{1-x-y}Be_xMg_ySe$ crystals [31,32]. Stronger exciton-phonon coupling for the Be/Mg-containing mixed crystals was explained by the poorer crystalline quality of the Be/Mg incorporated samples and compositional disorder in such quaternary solid solutions.

$Zn_{1-x}Be_xSe$ alloy is very interesting material. There is unusually large contrast in the physical properties of its bonds: Zn-Se, ionic, soft, long, a typical for II-VI and second one Be-Se, more III-V like: covalent, stiff and short [33]. Consequently, this fact leads to lattice hardening in beryllium containing crystals [13]. Firszt [13] et al. and Paszkowicz with co-workers [34] reported rapid microhardness increase in $Zn_{1-x}Be_xSe$ compounds with increasing x . They observed increase of microhardness caused by beryllium substitution by the factor 2.37 as compared to that of a binary ZnSe crystal. On the other hand, Firszt [13] observed in PL spectrum of $Zn_{1-x}Be_xSe$ crystals at $T=40$ K among others edge emission band. The well resolved LO-phonon structure in edge emission for low Be concentration was clearly visible and disappeared for high concentration due to increasing of alloy disorder with increasing beryllium content. Firszt et al. have found also several types of defects in $Zn_{1-x}Be_xSe$ alloy [35]. They have identified the stacking faults, misfit, edge, Frank and Shockley dislocations. It was established that the concentration of stacking faults increases with increasing beryllium content. It has been found also that quaternary $Zn_{1-x-y}Be_xMg_ySe$ crystals exhibit better luminescence efficiency and lower concentration of dislocations than $Zn_{1-x}Be_xSe$ ones. Results obtained in this work also confirm this fact. Looking back in Table 2 one can find that thermal conductivity value of $Zn_{0.72}Be_{0.06}Mg_{0.22}Se$ sample is comparable with obtained for $Zn_{0.74}Be_{0.26}Se$ crystal and even higher than for $Zn_{0.78}Mg_{0.22}Se$ alloy.

Defect characterization of ternary $Zn_{1-x}Be_xSe$ compound semiconductors was studied also by positron lifetime and photoluminescence measurements in [36]. The authors proved that the bulk lifetime of free positrons decreases with Be content, and consequently the concentration of vacancies was increasing. A comparison of positron measurements with theoretical calculations and photoluminescence experiments indicated that observed vacancies corresponded to a Be type vacancy.

As a conclusion of this section one can say, that there is no doubt that lattice disorder for mixed $Zn_{1-x-y}Be_xMg_ySe$ compounds increases in the investigated range of the composition.

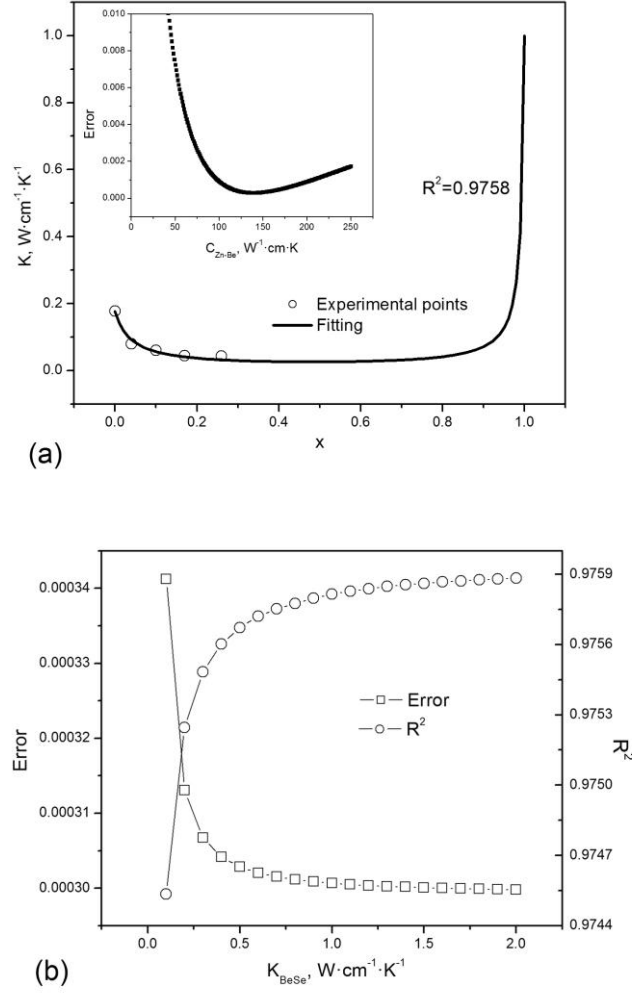


Fig. 4 Thermal conductivity K vs composition x for $\text{Zn}_{1-x}\text{Be}_x\text{Se}$ alloy (a). The open circles represent the experimental data and solid line is best fit obtained from Eq. (14) with parameter $C_{\text{Zn-Be}} = 139 \text{ W}^{-1} \cdot \text{cm} \cdot \text{K}$ and $K_{\text{BeSe}} = 1 \text{ W} \cdot \text{cm}^{-1} \cdot \text{K}^{-1}$ applying least square method. Error arising from fitting procedure is also given in inset. Picture (b) presents error and determination coefficient R^2 vs K_{BeSe} parameter for $C_{\text{Zn-Be}} = 139 \text{ W}^{-1} \cdot \text{cm} \cdot \text{K}$.

The electron contribution to the thermal conductivity in case of wide-gap II-VI crystals is very small indicating that the heat is mainly carried by phonons [28]. Therefore, the thermal conductivity of the crystal can be related only to the lattice contribution. Fig. 4 (a) presents the thermal conductivity $K(x)$ as a function of composition at room temperature for selected $\text{Zn}_{1-x}\text{Be}_x\text{Se}$ alloys. Best fit of Eq. (14) applying least square method was obtained for following parameter values: $C_{\text{Zn-Be}} = 139 \text{ W}^{-1} \cdot \text{cm} \cdot \text{K}$ and $K_{\text{BeSe}} = 1 \text{ W} \cdot \text{cm}^{-1} \cdot \text{K}^{-1}$. Determination coefficient R^2 indicating the quality of the fitting procedure was equal 0.9758. Similar results were obtained for $\text{Zn}_{1-x}\text{Mg}_x\text{Se}$ alloy, where $C_{\text{Zn-Mg}} = 116 \text{ W}^{-1} \cdot \text{cm} \cdot \text{K}$. Parameters $C_{\text{Zn-Be}}$ and $C_{\text{Zn-Mg}}$ describe contribution arising from the lattice disorder and are 2-6 times larger than obtained by Adachi for typical III-V ternary compounds [25]. However, the character of the change of the lattice thermal conductivity is in principal similar. One can observe rapid decrease and increase of the thermal conductivity for x value close to 0 and 1, respectively. Meanwhile in the middle of the graph there is plateau. Fig. 4 (b) presents error of

the fitting and the determination coefficient R^2 as the function of K_{BeSe} parameter for given value $C_{Zn-Be} = 139 \text{ W}^{-1} \cdot \text{cm} \cdot \text{K}$. One can see that there is no minimum with respect to K_{BeSe} values. Pure beryllium selenide (also magnesium selenide) does not exist in nature. Practically there are no experimental data for these binary crystals. However some theoretical predictions can be found, also for thermal properties. Lindsay et al. [37] calculated the thermal conductivity of the BeSe crystal as about $1 \text{ W} \cdot \text{cm}^{-1} \cdot \text{K}^{-1}$. This is rather typical value for III-V group and is almost 6 times more than in case of ZnSe. That confirms our statement about unusual contrast of $\text{Zn}_{1-x}\text{Be}_x\text{Se}$ alloy in comparison with other II-VI compounds. Unfortunately, no such data were found for MgSe binary crystal.

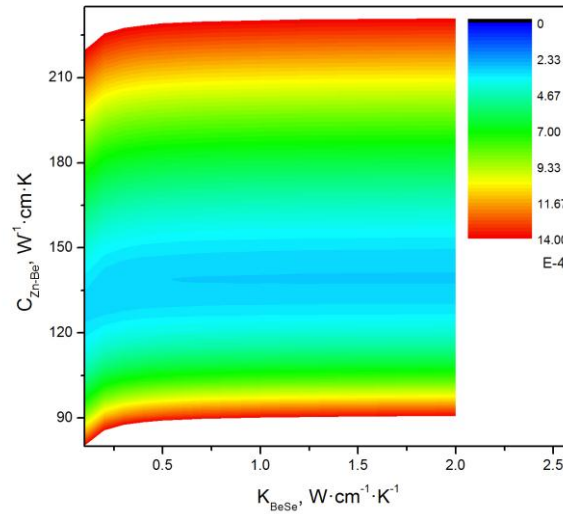


Fig. 5 Contour map of the error from two parameter (C_{Zn-Be} and K_{BeSe}) fitting procedure with least square method

More details concerning fitting can be found in Fig. 5. This picture shows contour map of the precision of the fitting varying two parameters (C_{Zn-Be} and K_{BeSe}). For each integer value of C_{Zn-Be} from the range 85 to 225 $\text{W}^{-1} \cdot \text{cm} \cdot \text{K}$ full scan of K_{BeSe} parameter was performed from 0 to 2 $\text{W} \cdot \text{cm}^{-1} \cdot \text{K}^{-1}$ with 0.1 single step. One can see that error arising from least square method is minimized vertically producing well determined value of C_{Zn-Be} . Despite there is no minimum indicating K_{BeSe} parameter, it does not influence obtained C_{Zn-Be} value. The author has tested the model given by Adachi for some hypothetical situation with known thermal conductivity of $\text{Zn}_{0.2}\text{Be}_{0.8}\text{Se}$ alloy. In such a case a minimum starts to be visible on the contour map returning fitted thermal conductivity value of pure BeSe binary crystal. It is known that in Bridgman vertical method there is change of the composition along growth axis, also in case of $\text{Zn}_{1-x}\text{Be}_x\text{Se}$ and $\text{Zn}_{1-x}\text{Mg}_x\text{Se}$ alloys. Exploiting this fact it is planned to verify what is the limit of the Be and Mg content in such compounds.

6 Conclusions

Investigated in this work mixed crystals were obtained with modified vertical Bridgman method. For the determination of the thermal parameters of the specimens photopyroelectric calorimetry has been applied. Measurements were performed in both, back and front detection

configurations, giving thermal diffusivity and effusivity values, respectively. Thermal conductivity of the investigated specimens was calculated from the relations between thermal parameters. Pure ZnSe binary crystal was used as test material. Obtained value of thermal conductivity of reference sample was in reasonable agreement with literature data. From the experimental results for mixed crystals concluded that increasing content of beryllium and magnesium lead to decreasing of value of all thermal parameters. It was shown that this effect is mainly due to increasing of lattice disorder in mixed semiconductor alloys. Crystal imperfections in such materials become scattering center for phonons leading to reducing of the ability of the material to conduct the heat. Obtained experimental results were also analyzed using model proposed by Adachi. Despite the lack of the experimental data of the BeSe and MgSe thermal conductivity fitting procedure was processed successfully. It was shown that parameters describing contribution to the thermal resistivity of the mixed compounds arising from the lattice disorder obtained for $Zn_{1-x}Be_xSe$ and $Zn_{1-x}Mg_xSe$ compounds were 2-6 times larger than in case of typical III-V alloys.

References

- [1] K.M. Yu, M.A. Mayer, D.T. Speaks, H. He, R. Zhao, *J. Appl. Phys.* 111 (2012) 123505.
- [2] A. Shen, A.P. Ravikumar, G. Chen, K. Zhao, A. Alfaro-Martinez, T. Garcia, J. de Jesus, M.C. Tamargo and C. Gmachl, *J. Vac. Sci. Technol. B* 31 (2013) 03C113.
- [3] Y.N. Hou, Z.X. Mei, H.L. Liang, D.Q. Ye, C.Z. Gu and X.L. Du, *Appl. Phys. Lett.* 102 (2013) 153510.
- [4] M. Niraula, K. Yasuda, H. Yamashita, Y. Wajima, Y. Tsukamoto, M. Matsumoto, Y. Suzuki, N. Takai, Y. Tsukamoto and Y. Agata, *Phys. Status Solidi C* 11 (2014) 1333.
- [5] P. Wojnar, E. Janik, L.T. Baczewski, S. Kret, E. Dynowska, T. Wojciechowski, J. Suffczyński, J. Papierska, P. Kossacki, G. Karczewski, J. Kossut, T. Wojtowicz, *Nano Lett.* 12(7) (2012) 3404.
- [6] L. Xiao, D. Mei, M. Cao, D. Qu, B. Deng, *J. Alloy. Compd.* 627 (2015) 455.
- [7] A.P. Ravikumar, T.A. Garcia, J. de Jesus, M. Tamargo, and C. Gmachl, *Appl. Phys. Lett.* 105 (2014) 061113.
- [8] D. Trefon-Radziejewska, J. Bodzenta, *Opt. Mater.* 45 (2015) 47.
- [9] D. Korte, E. Paclica, G. Bratina, M. Franko, *Int. J. Thermophys.* 35 (2014) 1990.
- [10] M. Pawlak, M. Maliński, *Thermochim. Acta* 599 (2015) 23.
- [11] D. Dadarlat, M.N. Pop, M. Streza, S. Longuemart, M. Depriester, A. Hadj Sahraoui and V. Simon, *Int. J. Thermophys.* 31 (2010) 2275.
- [12] S. Adachi, *J. Appl. Phys.* 102 (2007) 063502.
- [13] F. Firszt, S. Łęgowski, H. Męczyńska, J. Szatkowski, W. Paszkowicz and K. Godwod, *J. Cryst. Growth* 184/185 (1998) 1335.
- [14] Mala N. Rao, D. Lamago, A. Ivanov, M. d'Astuto, A. V. Postnikov, R. Hajj Hussein, Tista Basak, S. L. Chaplot, F. Firszt, W. Paszkowicz, S. K. Deb and O. Pagès, *Phys. Rev. B* 89 (2014) 155201.
- [15] F. Firszt, H. Męczyńska, B. Sekulska, J. Szatkowski, W. Paszkowicz and J. Kachniarz, *Semicond. Sci. Technol.* 10 (1995) 197.

- [16] F. Firszt, J. Zakrzewski K. Strzałkowski, M. Maliński, S. Łęgowski, H. Męczyńska, A. Marasek, Y.S. Huang and D. Dumcenco, *Phys. Status Solidi C7* (2010) 1463.
- [17] K. Strzałkowski, M. Streza, M. Pawlak, *Measurement* 64 (2015) 64.
- [18] K. Strzałkowski, D. Dadarlat, M. Streza, F. Firszt, *Thermochim. Acta* (2015) DOI: 10.1016/j.tca.2015.06.027.
- [19] A. Mandelis and M.M. Zver, *J. Appl. Phys.* 57 (1985) 4421.
- [20] M. Chirtoc and G. Mihailescu, *Phys. Rev. B* 40 (1989) 9606.
- [21] D. Dadarlat, *Laser Phys.* 19 (2009) 1330.
- [22] J. Morimoto, Y. Okamoto and T. Miyakawa, *Jpn. J. Appl. Phys.* 31 (1992) 38.
- [23] Y. Okamoto, R. Okada, T. Nemoto, H. Ohta, H. Takiguchi, *Int. J. Thermophysics.* 33 (2012) 1219.
- [24] B. Abeles, *Phys. Rev.* 131 (1963) 1906.
- [25] S. Adachi, *J. Appl. Phys.* 54 (1983) 1844.
- [26] D. Dadarlat, M. Streza, M.N. Pop, V. Tosa, S. Delenclos, S. Longuemart, A. Hadj Sahraoui, *J. Therm. Anal. Calorim.* 101 (2010) 397.
- [27] O. Madelung, *Semiconductors: Data Handbook*, Springer, Berlin, Heidelberg, 2003.
- [28] G. Slack, *Phys. Rev. B* 6 (1972) 3791.
- [29] K. Strzałkowski, *Mater. Sci. Eng. B* 184 (2014) 80.
- [30] D. O. Dumcenco, Y.S. Huang, H.P. Hsu, K. Tiong, F. Firszt, K. Strzałkowski, S. Łęgowski, H. Męczyńska, *J. Appl. Phys.* 108 (2010) 053502-1.
- [31] D. O. Dumcenco, Y.S. Huang, F. Firszt, S. Łęgowski, H. Męczyńska, A. Marasek, K. Strzałkowski, W. Paszkowicz, K. K. Tiong, C. H. Hsieh, *J. Appl. Phys.* 104 (2008) 073528.
- [32] D.O. Dumcenco, Y.M. Chen, Y.S. Huang, F. Firszt, S. Łęgowski, H. Męczyńska, A. Marasek, K.K. Tiong, *J. Alloy. Compd.* 491 (2010) 472.
- [33] T. Ganguli, J. Mazher, A. Polian, S.K. Deb, F. Villain, O. Pages, W. Paszkowicz, F. Firszt, *J. Appl. Phys.* 108 (2010) 083539-1.
- [34] W. Paszkowicz, K. Godwod, J. Domagała, F. Firszt, J. Szatkowski, H. Męczyńska, S. Łęgowski and M. Marczak, *Solid State Commun.* 107 (1998) 735.
- [35] F. Firszt, S. Łęgowski, H. Męczyńska, J. Szatkowski, A. Banasiak, W. Paszkowicz, U. Falke, S. Schulze, M. Hietschold, *J. Cryst. Growth* 214/215 (2000) 880.
- [36] F. Plazaola, J. Flyktman, K Sarinen, L. Dobrzyński, F. Firszt, S. Łęgowski, H. Męczyńska, W. Paszkowicz, H. Reniewicz, *J. Appl. Phys.* 91 (2003) 1647.
- [37] L. Lindsay, D.A. Broido and T.L. Reinecke, *Phys. Rev. B* 88 (2013) 144306.